Design of a High-Speed Ethernet Connector for Harsh Environments

Younes Boujmad, Cédric Bermond, Philippe Artillan, Olivier Gavard, Marie Prudhom, Farsin Khalili, Edith Husson-Charlet, Jean-Paul Barbosa, Bernard Flechet

Design of a high Speed Ethernet Connector for Harsh Environments

Younes BOUJMAD, Cédric BERMOND, Philippe ARTILLAN, Olivier GAVARD, Marie PRUDHOM, Farsin KHALILI, Edith HUSSON CHARLET, Jean-Paul BARBOSA, Bernard FLECHET

***Abstract*—This paper focuses on the electrical performance of a new Ethernet contact with four differential pairs called "Octomax". The eight pins of the contact are inserted on a section of 17 mm^2. Such a high speed interconnect solution is especially developed to operate at 10 Gbits/s in harsh environments for military and aerospace applications. The theoretical study up to 1 GHz enables quantifying the crosstalk between two differential pairs (NEXT), the return loss (RL) and the insertion loss (IL). An optimization using a combined 2D-3D electromagnetic approach, which is simultaneously validated by measurement in frequency and time domains, leads to a final prototype that meets the category 6A Ethernet standard for predictable data rate of 10 Gbits/s.**

***Index Terms*—category 6A, contact, coupling coefficient, electromagnetic modeling, high speed Ethernet, Octomax.**

I. Introduction

Developing high speed connectors [1] is one of the greatest challenges for harsh environments. Military and aerospace applications require specific constraints for connectors [2], such as high tolerance for vibrations (up to 20g), wideband temperatures (between -65°C and 200°C), weight and miniaturization. For high-speed Ethernet link, lower power consumption and excellent EMI compatibility, the Quadrax contacts are already qualified [3], allowing maximum data rates of 1 Gbits/s. Theses contacts are composed of four pins. Therefore it is necessary to use two Quadrax contacts to connect an Ethernet network cable. The RJ45 connectors are excluded from this type of applications since they do not respect the thermal, mechanical and corrosion stresses.

The development of new electrical contacts with increased data rates passes necessary through increasing the number of pins. Accordingly, we propose a new contact named "Octomax" that integrates four differential pairs (eight pins) into the same Quadrax cavity (miniaturization issue) and specified to achieve 10 Gbits/s. Therefore the contact must meet the category 6A hardware Ethernet standards, extracted from the 10GBASE-T ISO/IEC 11801 standard [4]. As the four differential pairs transmit data using a baseband digital transmission (PAM 16/DSQ 128) [5], these category 6A standards specify limits up to 500 MHz, for the insertion loss or IL (inline attenuation), return loss or RL (impedance mismatch) and the near-end crosstalk or NEXT (electromagnetic crosstalk between differential pairs). At the highest frequencies, the RL and the NEXT become predominant and degrade the electrical performance of the contacts. Crosstalk is particularly increased as the number of differential pairs is high. Therefore, compactness is a challenge for the implementation of these new contacts. Octomax is adapted to be mounted on cavity connectors for US military connectors standards (MIL-DTL-38999) and for European aeronautics connectors standards (EN3645) replacing the Quadrax contact (Fig. 1). They will have to respond to vibratory constraints (sinusoidal and random vibrations of 10 to 20 G per axis) and thermal constraints (wideband temperatures).

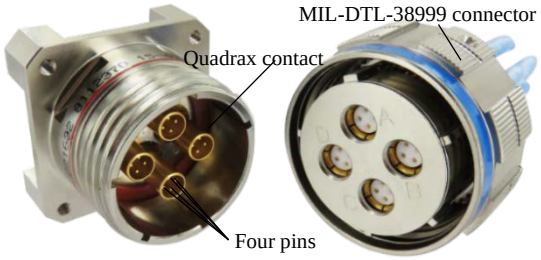

Fig. 1. MIL-DTL-38999 Quadrax connector (Amphenol-Socapex)

This paper is organized as follows. Section II describes the Octomax contact structure. Section III presents a theoretically study of two differential coupled line which allow to express the NEXT for different values of coupling coefficients. Section IV presents electrical performances of a first prototype and allows the co-validation of measurement and simulation tools. An optimized contact is finally proposed, analyzed and measured in section V.

II. Octomax: Description

The Octomax contact is made up of a male part and a female part which once connected form a 6 cm long contacts pair. The eight central pins (4 differential pairs) are held in a dielectric material formed from a thermoplastic polymer of low permittivity which can withstand very high temperature (up to 200°C). A cylindrical metal external envelop with an outside diameter around 5.7 mm is the ground plane reference of the contact. This envelope also ensures the mechanical holding of the central male and female part when coupled together. The pins and the cavity are based on a copper alloy and then gold

This work was supported by the Région Auvergne-Rhône-Alpes, France.

Y. Boujmad, P. Artillan, C. Bermond and B. Fléchet are with University Savoie Mont-Blanc, IMEP-LAHC, UMR CNRS 5130, 73376 Le Bourget du Lac, France (e-mail: younes.boujmad@univ-smb.fr, philippe.artillan@univ-smb.fr, cedric.bermond@univ-smb.fr)

O.Gavard, M.Prudhom, F.Khalili, E.Husson-Charlet and J-P.Barbosa are with Amphenol Socapex, 948 Prom de l'Arve, 74300 Thyez, France

over nickel plated by electrodeposition.

Two prototypes were developed. The first prototype named Octomax 1.0 was intended to minimize the crosstalk between the differential pairs and was then designed with a metal shield cross inserted between four homogenous dielectric pieces in both parts of the contact as shown in Fig 2.

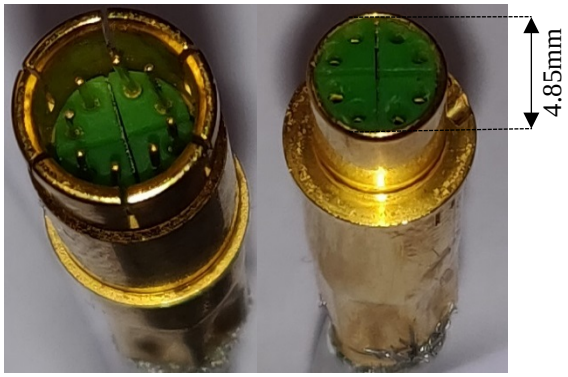

Fig. 2. Female and male part of the first prototype: Octomax 1.0

The optimization of the first prototype led to a second prototype named Octomax 2.0. This contact has an inhomogeneous dielectric material and four metal plates inserted between differential pairs, as described in section V.

The dielectric part of these two prototypes was realized with 3D printed polymer, whereas in an industrial context, it will be made of thermo-injected polymer.

III. Theoretical Study for Two Coupled Differential Pairs

Octomax contact has four pairs with differential excitations. The category 6A Ethernet standard describes three criteria guarantying signal integrity: insertion loss (IL), return loss (RL) and near-end crosstalk (NEXT). Fig. 3 defines those values for pair 1-5, RL is the reflection on differential port 1, IL is the transmission between ports 1 and 5 and NEXT is defined between ports 1 and 2.

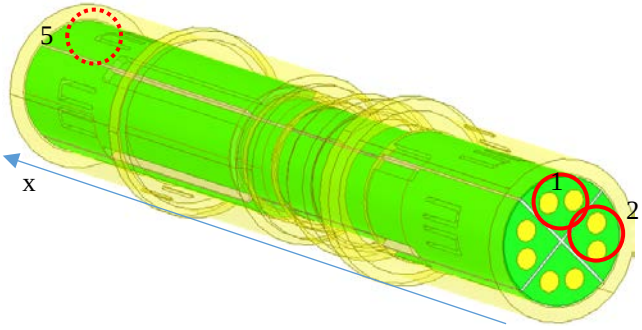

Fig. 3. 3D view of the Octomax 1.0

In this part we will estimate theoretically the electromagnetic crosstalk (NEXT) from a simple case of two lossless and identical differential pairs. The equivalent diagram of two coupled differential pairs is given in Fig. 4, where $L_0{}'$, $C_0{}'$ are respectively self-inductance and self-capacitance per unit length of a differential pair. The magnetic induction between two differential pairs is described by the mutual inductance L_m

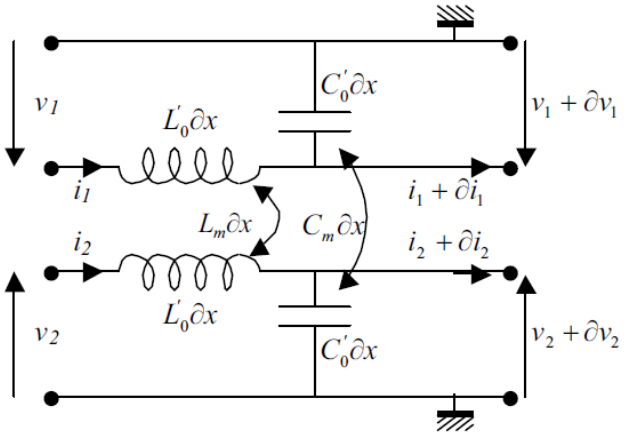

Fig. 4. Two coupled differential pairs distributed cell

and the electrical coupling by the mutual capacitance C_m. Defining: $C = C_m + C_0{}'$ and $L = L_0{}'$, the Kirchhoff equations for the case of two lossless coupled differential pairs is described by the following equations:

$$\begin{cases} -\dfrac{\partial v_1}{\partial x} = j\omega(Li_1 + L_m i_2) \\ -\dfrac{\partial v_2}{\partial x} = j\omega(L_m i_1 + Li_2) \\ -\dfrac{\partial i_1}{\partial x} = j\omega(Cv_1 - C_m v_2) \\ -\dfrac{\partial i_2}{\partial x} = j\omega(-C_m v_1 + Cv_2) \end{cases} \quad (1)$$

The general solution is built from a superposition of two normal modes. Expressing the solutions for identical differential pairs, both normal modes become the even and odd modes [6]. We define for both even and odd modes the voltage and the current [7] as:

$$\begin{cases} v_e = \dfrac{v_1 + v_2}{2} \\ v_o = \dfrac{v_1 - v_2}{2} \end{cases} \quad (2)$$

$$\begin{cases} i_e = \dfrac{i_1 + i_2}{2} \\ i_o = \dfrac{i_1 - i_2}{2} \end{cases} \quad (3)$$

The capacitive and inductive coupling coefficients are given by (4)

$$\begin{cases} k_L = \dfrac{L_m}{L} \\ k_C = \dfrac{C_m}{C} \end{cases} \quad (4)$$

From previous set of equations, we obtained the following equations for even and odd propagation modes.

$$\begin{cases} -\dfrac{\partial v_e}{\partial x} = jL\omega i_e(1 + k_L) \\ -\dfrac{\partial i_e}{\partial x} = jC\omega v_e(1 - k_C) \\ -\dfrac{\partial v_o}{\partial x} = jL\omega i_o(1 - k_L) \\ -\dfrac{\partial i_o}{\partial x} = jC\omega v_o(1 + k_C) \end{cases} \quad (5)$$

Taking the derivative of (5), we deduce the propagation

equations of even and odd modes:

$$\begin{cases} \frac{\partial^2 v_e}{\partial x^2} + LC(1+k_L)(1-k_C)\omega^2 v_e = 0 \\ \frac{\partial^2 v_O}{\partial x^2} + LC(1-k_L)(1+k_C)\omega^2 v_o = 0 \\ \frac{\partial^2 i_e}{\partial x^2} + LC(1+k_L)(1-k_C)\omega^2 i_e = 0 \\ \frac{\partial^2 i_O}{\partial x^2} + LC(1-k_L)(1+k_C)\omega^2 i_o = 0 \end{cases} \quad (6)$$

The solutions of both modes separately are represented as:

$$\begin{cases} v_e = v_e{}^+ + v_e{}^- = A_1 e^{-j\beta_e x} + A_2 e^{+j\beta_e x} \\ v_o = v_o{}^+ + v_o{}^- = A_3 e^{-j\beta_o x} + A_4 e^{+j\beta_o x} \end{cases} \quad (7)$$

$$\begin{cases} i_e = i_e{}^+ - i_e{}^- = \frac{A_1}{Zc_e} e^{-j\beta_e x} + \frac{A_2}{Zc_e} e^{+j\beta_e x} \\ i_o = i_o{}^+ - i_o{}^- = \frac{A_3}{Zc_o} e^{-j\beta_o x} + \frac{A_4}{Zc_o} e^{+j\beta_o x} \end{cases} \quad (8)$$

The phase constants β_e, β_o for both even and odd modes are then expressed as:

$$\beta_e = \omega\sqrt{LC(1+k_L)(1-k_C)} \quad (9)$$

$$\beta_o = \omega\sqrt{LC(1-k_L)(1+k_C)} \quad (10)$$

The characteristic impedance Zc_e, Zc_o can be defined as the ratio of the voltage to the current of a single wave, travelling in one direction in the absence of reflections in the opposite direction, of the corresponding mode. By expressing voltage as a function of the current in equation (5), we obtain:

$$Zc_e = \frac{v_e{}^+}{i_e{}^+} = \sqrt{\frac{L}{C}}\sqrt{\frac{1+k_L}{1-k_C}} \quad (11)$$

$$Zc_o = \frac{v_o{}^+}{i_o{}^+} = \sqrt{\frac{L}{C}}\sqrt{\frac{1-k_L}{1+k_C}} \quad (12)$$

From the phase constant and characteristic impedance we can express the scattering coefficients of both modes [8]:

$$S_{11e} = \frac{j\left(\frac{Zc_e}{Z_0} - \frac{Z_0}{Zc_e}\right)sin\theta_e}{2cos\theta_e + j\left(\frac{Zc_e}{Z_0} + \frac{Z_0}{Zc_e}\right)sin\theta_e} \quad (13)$$

$$S_{21e} = \frac{2}{2cos\theta_e + j\left(\frac{Zc_e}{Z_0} + \frac{Z_0}{Zc_e}\right)sin\theta_e} \quad (14)$$

$$S_{11o} = \frac{j\left(\frac{Zc_o}{Z_0} - \frac{Z_0}{Zc_o}\right)sin\theta_o}{2cos\theta_o + j\left(\frac{Zc_o}{Z_0} + \frac{Z_0}{Zc_o}\right)sin\theta_o} \quad (15)$$

$$S_{21o} = \frac{2}{2cos\theta_o + j\left(\frac{Zc_o}{Z_0} + \frac{Z_0}{Zc_o}\right)sin\theta_o} \quad (16)$$

With: $\begin{cases} \theta_e = \beta_e l \\ \theta_o = \beta_o l \end{cases}$ phase shift between the incident wave and the emergent wave for even and odd modes, l: the physical length of a differential pair and $Z_0 = 100\ \Omega$ is the normalized impedance of the port.

The three criteria are calculated from the reflection and transmission coefficients of both modes:

$$-NEXT = 20log_{10}\left(\left\|\frac{S_{11e} - S_{11o}}{2}\right\|\right) \quad (17)$$

$$-RL = 20log_{10}\left(\left\|\frac{S_{11e} + S_{11o}}{2}\right\|\right) \quad (18)$$

$$-IL = 20log_{10}\left(\left\|\frac{S_{21e} + S_{21o}}{2}\right\|\right) \quad (19)$$

We take: $\sqrt{LC} = \frac{\sqrt{\varepsilon_r}}{3.10^8} = 6.06\ ns/m$ and $\sqrt{\frac{L}{C}} = 100\Omega$ which values correspond to the nominal set of two uncoupled lines and we suppose that the coupling is weak enough in the following study. Furthermore, in homogeneous case, the capacitive coupling coefficient is equal to the inductive coupling coefficient. We seek the maximum value of coupling coefficient in order to respect the category 6A crosstalk specification. The value of the NEXT is calculated as a function of frequency for different values of coupling coefficient (Fig. 5).

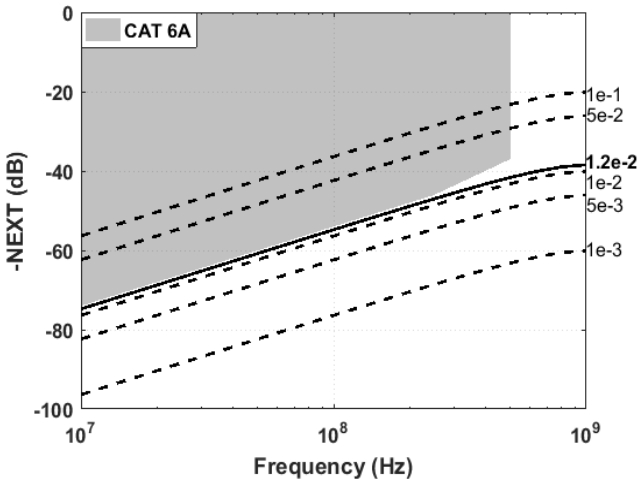

Fig. 5. Theoretical crosstalk between two differential pairs as a function of the capacitive and inductive coupling coefficient k.

As a result, for category 6A crosstalk specification, the capacitive and inductive coupling coefficients should be lower than $1.2.10^{-2}$. As the spacing between the pairs is standardized, it is necessary to insert a shielding between the differential pairs. The next part will expound the measurement and simulation of a structure fully shielded by a metal cross.

IV. OCTOMAX 1.0

A. Validation of measurement and simulation tools

An electromagnetic modeling tool has been especially developed. It consists in representing the contact as seven cascaded segments, since the geometry of the contact varies along its length as shown in Fig 6-(a). The differences between segments are the variations of the diameter of the pins, the diameter of the dielectric (represented in green color) and the internal diameter of the metallic cavity. Note that only in segment 4, there is no dielectric and no shielding cross.

For each segment, the structure is considered as 8 coupled transmission lines. The segments are all modeled under ANSYS 2D Extractor solver (Fig 6-(b)).

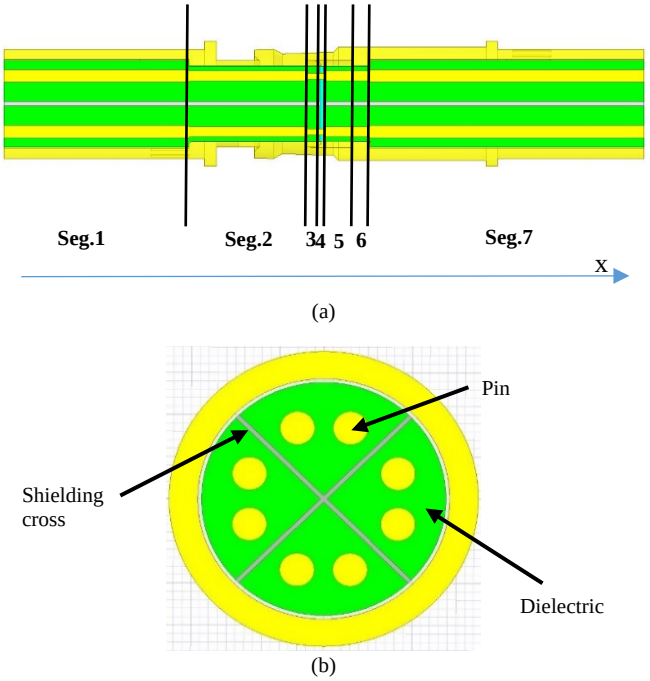

Fig. 6-(a) Cross section of the Octomax 1.0 contact with seven segments; (b) First segment modeled under ANSYS 2D Extractor.

The distributed RLCG matrix from the 2D simulation, and the length of each segment are used to generate the corresponding ABCD matrix [9]. Using the cascading property of ABCD matrix, we calculate the ABCD matrix of the contact and then generate the single-ended S matrix S_{se} [10] of the contact. The differential-mode matrix S_{dd} is then deducted using the mixed-mode conversion from the following equations:

$$S_{mm} = P_{mm} S_{se} {P_{mm}}^{-1} \tag{20}$$

$$P_{mm} = \begin{bmatrix} \frac{1}{\sqrt{2}} & -\frac{1}{\sqrt{2}} & 0 & 0 & \dots & 0 & 0 & 0 \\ 0 & 0 & \frac{1}{\sqrt{2}} & -\frac{1}{\sqrt{2}} & 0 & 0 & \dots & 0 \\ \vdots & \vdots & \vdots & \vdots & \ddots & \ddots & 0 & 0 \\ 0 & 0 & 0 & 0 & 0 & 0 & \frac{1}{\sqrt{2}} & -\frac{1}{\sqrt{2}} \\ \frac{1}{\sqrt{2}} & \frac{1}{\sqrt{2}} & 0 & 0 & \dots & 0 & 0 & 0 \\ 0 & 0 & \frac{1}{\sqrt{2}} & \frac{1}{\sqrt{2}} & 0 & 0 & \dots & 0 \\ \vdots & \vdots & \vdots & \vdots & \ddots & \ddots & 0 & 0 \\ 0 & 0 & 0 & 0 & 0 & 0 & \frac{1}{\sqrt{2}} & \frac{1}{\sqrt{2}} \end{bmatrix}_{16X16}$$

$$S_{mm} = \begin{bmatrix} S_{dd} & S_{dc} \\ S_{cd} & S_{cc} \end{bmatrix}_{16X16}$$

Where P_{mm} is the conversion matrix from the single ended to the mixed-mode S_{mm}, S_{dd} is the differential mode S-parameters matrix, S_{cc} is the common mode S-parameters matrix, S_{dc} and S_{cd} are the cross-mode S-parameters matrix. In particular S_{dc} describes the coupling between the common-mode and the differential-mode. However the contact has a symmetric structure which theoretically produces no cross-mode. The simulation of cross-mode coupling confirms that its contribution is negligible. We will more precisely focus on the differential mode matrix S_{dd}.

In parallel, the contact was simulated in the [10 MHz, 1 GHz] bandwidth using ANSYS HFSS 3D full wave solver. Measurements of the first prototype of the contact are presented and used to validate the employed modeling methods. In order to move the measurements reference planes to the ends of the contact, thus enabling measurements in the same conditions as simulations, the measurements have been de-embedded with a specific procedure. The results have been obtained by first calibrating up to the SMA ends of the cables with automatic SOLT 4 ports calibration and then by a 1-port SOL de-embedding procedure on each port (considering no coupling between ports on the well shielded test fixture). The contact has been tested with 4-ports Keysight PNAX5247A in several configurations to characterize reflection ($S11_{dd}$), transmission ($S51_{dd}$) and crosstalk ($S21_{dd}$). The 2D and 3D simulation results were then confronted with VNA measurement results up to 1 GHz and with regard to the category 6A Ethernet standards as shown in Fig 7.

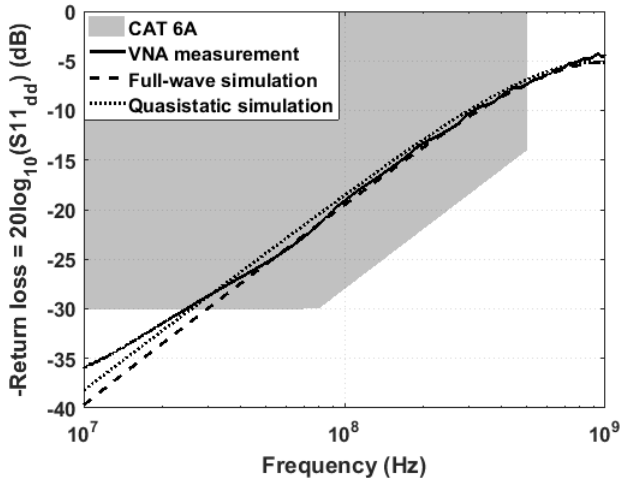

(a)

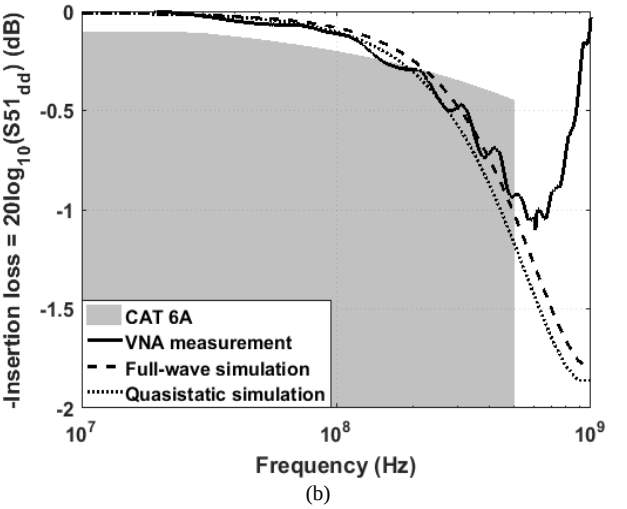

(b)

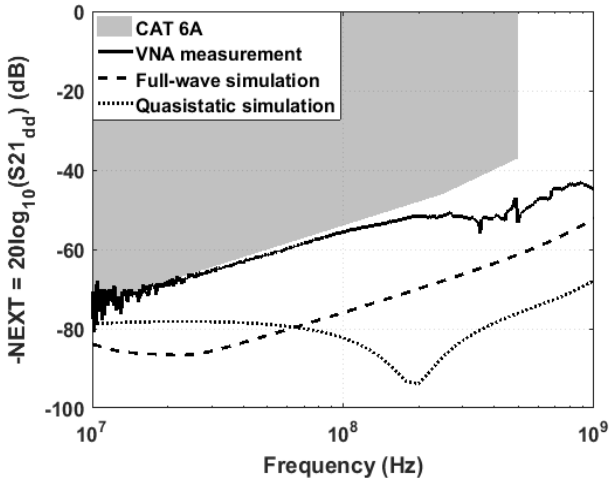

(c)

Fig 7. Results of the 2D approach and 3D full wave simulation compared with VNA measurement for the first prototype. (a) Return loss; (b) Insertion loss; (c) NEXT.

The RL and IL results (Fig.7-(a), (b)) obtained by the 2D segmentation approach are equivalent to the 3D full wave simulation from HFSS. These two results were confirmed by VNA measurement. The de-embedding procedure leads to measurement uncertainty at high frequency, as visible on insertion loss curve in Fig. 7-(b). The 2D approach allows faster computing for pre-optimization and 3D approach gives excellent predictions of electrical performances of the contact for IL and RL. The evaluation of the NEXT (Fig.7-(c)) is an especially hard task, as the levels are very low but quite good agreement between the two modeling methods is obtained. The measured NEXT appears higher than the simulated NEXT, probably because of remaining coupling between pairs due to the imperfect de-embedding of the connection system. An improved test fixture, with better differential impedance matching, will be implemented in the future to allow better measurements. Next part presents the electrical performances of the contact compared to category 6A expectations.

B. Electrical specifications of Octomax 1.0

The RL level (Fig.7-(a)) of each differential pair is 8.5 dB higher than the value imposed by the Ethernet category 6A standard. This is due to the impedance mismatch of each differential pair (different from 100 Ω). The degradation of the IL, as presented in Fig.7-(b), is also mainly due to the impedance mismatch which attenuates the transmitted signal. The Octomax 1.0 therefore does not meet the category 6A Ethernet standards. For further investigation, a measurement of the characteristic impedance along the differential pair contact has been performed using the Tektronix CSA 803 TDR bench. In fact the TDR emits a differential step voltage of 500 mV amplitude with a rise time of less than 25 ps. It then calculates the characteristic impedance from an analysis of the reflected signal versus the transmitted signal.

A fluctuating value ranged between 60 Ω and 70 Ω is observed, as shown in Fig. 8. This range is below our target value of 100 Ω for differential mode propagation.

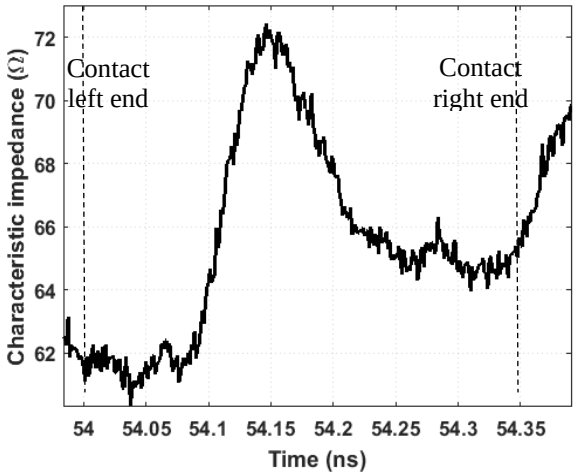

Fig 8. TDR measurement of the characteristic impedance of a differential pair along the contact

The increase in the number of pins, without any other modification of the design, has resulted in a reduction in the distances between the conductors and the ground plane (cylindrical cavity and the shielding cross). This high density of internal contacts (pins) has the consequence of increasing the self-capacitance of each differential pair, therefore reducing the differential characteristic impedance of the Octomax 1.0. The differential NEXT (Fig.7-(c)) is in accordance with the specification of the category 6A standards. Therefore, the metal cross enables good capacitive and inductive shielding. However, mounting the contact is made difficult because the dielectric is divided in four parts due to the metal cross. The goal would then be to increase the differential characteristic impedance of the contact in order to meet the category 6A Ethernet standards for RL and IL. Simultaneously, the metal cross shield that divides the dielectric into four pieces should be replaced by an already integrated shield that still passes the category 6A NEXT specification.

V. Optimized contact: Octomax 2.0

A. Optimization process

As the full-wave analysis is typically more complex and time consuming, the 2D concatenating method was used for optimization process. The industrial specifications locked several solutions for optimization, such as increasing the diameter of the body, changing the nature of the polymer and changing the location of the pins. The challenge then was to achieve good signal integrity of the contact with many technological locks but also taking into account the ease of assembly and the mechanical strength. Several modifications have been proposed and realized at first on 2D approach such as modifying the geometry of the dielectric surrounding the pins, the shape of the shielding and the diameter of the pins in some critical locations. Indeed, the ambition was to replace a shielding cross that separates the dielectric into four pieces by a new dielectric piece with air gaps molded in one piece with the shielding. In fact, the air gaps inserted in between the pins and between the body and the pins in some part of the contact,

reduces the effective permittivity. As the capacitive effect is proportional to the permittivity, the mutual and self-capacitances then decrease and the characteristic impedance increases. Further reducing the diameter of the pins leads to separate them and thus reduce the capacitive coupling between them and consequently increase the characteristic impedance. Fig. 9 shows the characteristic impedance of the optimized contact compared to the Octomax 1.0 contact as a function of the position over the contact in longitudinal direction.

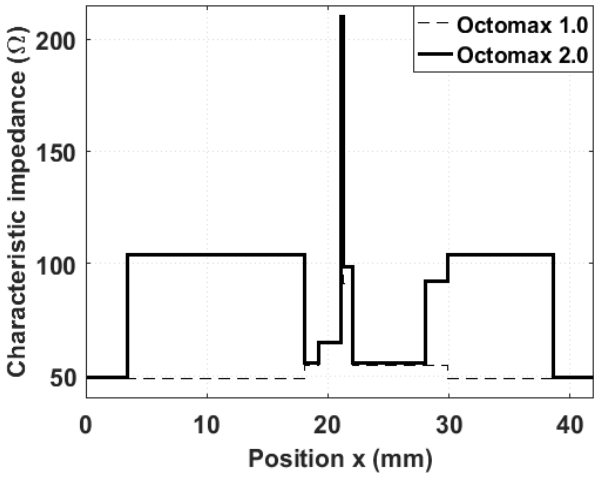

Fig 9. Differential impedance of the optimized contact compare to the first design as function of position over the contact in longitudinal direction.

These modifications allowed to increase the characteristic impedance of the differential pairs in the longest segments of the contact. Note that for mechanical strength constraints, optimizations have not been made throughout the contact.

A 3D model of the new optimized contact Octomax 2.0 as shown in figure 10 was simulated on HFSS from 10 MHz to 1 GHz designed for thermo-injection process.

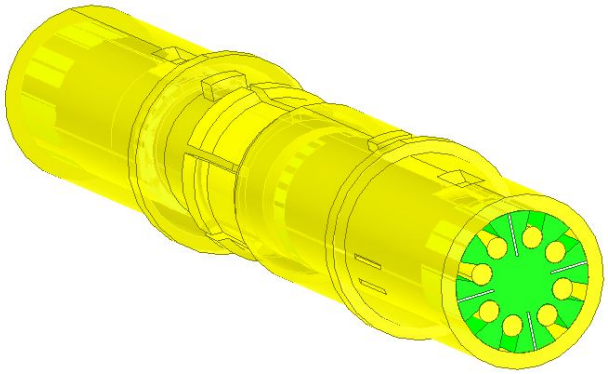

Fig. 10. 3D view of the Octomax 2.0

The performed simulation has led to the precise knowledge of the impedance mismatch and the crosstalk.

B. Impedance mismatch evaluation

The differential S_{dd} matrix is supposed to verify the properties of four coupled transmission lines. Under these assumptions, one can define the equivalent characteristic impedance matrix Zc_{eq} and the equivalent propagation constant matrix Γ_{eq} [11]. Furthermore, as all transmission lines are similar with each other, one can plot the first value of the diagonal of Zc_{eq} to evaluate the impedance mismatch (Fig. 11).

This computation has been applied on both prototypes Octomax 1.0 and Octomax 2.0.

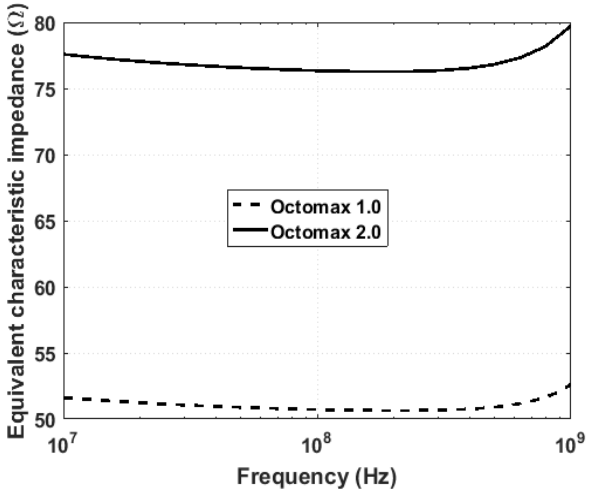

Fig. 11. Equivalent characteristic impedance of both structures of the contact

The equivalent characteristic impedance of the Octomax 1.0 is around 52 Ω. This low equivalent characteristic impedance was also previously measured in TDR measurement in section IV.

The characteristic impedance of the optimized contact Octomax 2.0 reaches 78 Ω, thus reducing the impedance mismatch with the 100 Ω standard.

C. Crosstalk evaluation

Crosstalk analysis will be done through capacitive and inductive coefficients. These coefficients are calculated from the RLCG parameters deducted from the matrices Zc_{eq} and Γ_{eq} defined in previous section.

$$L = \frac{1}{2\pi f} imag\left(sqrtm\left({\Gamma_{eq}}^2\left({Zc_{eq}}^2\right)^{-1}\right){Zc_{eq}}^2\right) \quad (21)$$

$$C = \frac{1}{2\pi f} imag\left(sqrtm\left({\Gamma_{eq}}^2\left({Zc_{eq}}^2\right)^{-1}\right)\right) \quad (22)$$

$$\begin{cases} k_L = \left|\frac{L_{12}}{\sqrt{L_{11}L_{22}}}\right| \\ k_C = \left|\frac{C_{12}}{\sqrt{C_{11}C_{22}}}\right| \end{cases} \quad (23)$$

An additional structure named unshielded Octomax is also simulated. This structure is designed from the first prototype but without the metal shield cross. Fig 12 shows the capacitive and inductive coupling coefficient of three simulated structures of contact.

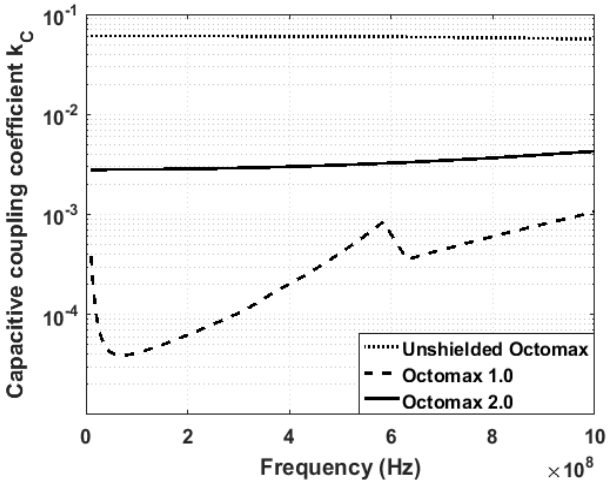

(a)

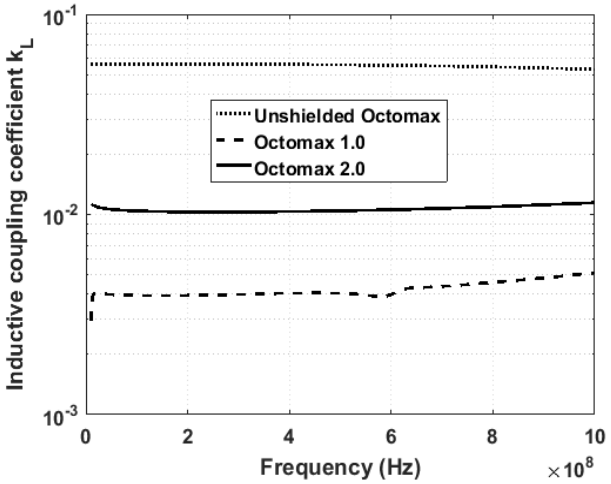

(b)

Fig. 12. Coupling coefficients as a function of frequency of three different structures of contact. (a) Capacitive coupling; (b) Inductive coupling.

In the case of unshielded Octomax, the capacitive and inductive coefficient, as shown in Fig. 12-(a), (b), are strictly equal ($k_C = k_L = 6.10^{-2}$), and higher than the maximum theoretical coupling coefficient tolerable to meet the category 6A ($1.2.10^{-2}$). These coupling coefficients lead to a high crosstalk level: 10 dB above the category 6A limitation, as it's shown in Fig. 5.

Conversely, a structure fully shielded by a metal cross (Octomax 1.0) has a low capacitive and inductive coupling coefficients compared to the tolerable coupling coefficient defined in section III such as $k_C = 2.10^{-4}$ and $k_L = 3.10^{-3}$, at 400 MHz, moreover $k_C < k_L$. Therefore the metal shielding considerably reduces the capacitive coupling compared to the inductive coupling.

In the case of the optimized contact (Octomax 2.0) the shielding is only partial with intermediate values of $k_C = 3.10^{-3}$ and $k_L = 10^{-2}$. Both coupling coefficients are below the minimum value required to meet the category 6A standard for crosstalk. Furthermore, the shielding of the differential pair has been sized to find the best compromise between crosstalk (NEXT enhancements) and impedance matching (RL). In addition to that, this new shielding is easier to insert in a single piece of inhomogeneous material.

D.Category 6A validation for Octomax 2.0

A preliminary prototype of the optimized contact has been realized with 3D printed dielectric material, thus partly proving the fabrication feasibility. Fig. 13-(a), (b), and (c) show simulation results of the new optimized contact Octomax 2.0 compared to VNA measurements and to the theoretical calculation from section III equations.

Both simulation and theoretical results show good agreement up to 1GHz. The measured return loss and insertion loss, as shown in Fig. 13-(a), (b), are in close agreement up to 500 MHz. The measured NEXT (Fig.13-(c)) is 10 dB higher than the simulated NEXT because of the additional coupling of the crimping part.

The RL is 10 dB lower, due to the increase of the characteristic impedance of differential pairs. The IL level was also improved through the optimization of the characteristic impedance. Thus increasing the characteristic impedance of the contact is of first importance in order to meet the RL and IL specification.

The crosstalk has been increased but remains in the limits of the specification of category 6A. The new contact Octomax 2.0 meets the category 6A Ethernet requirements for a bit rate of 10 Gbits/s.

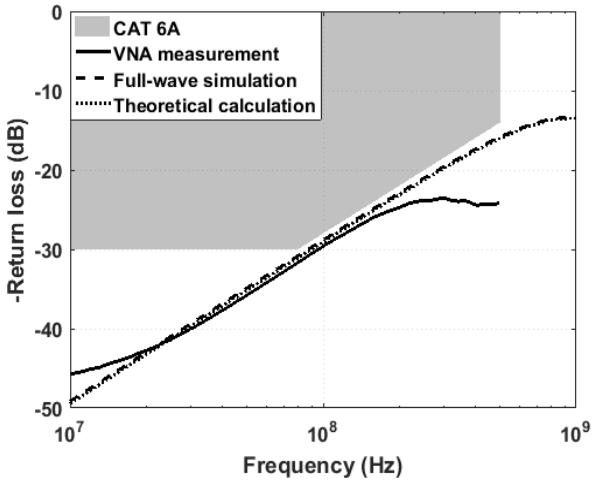

(a)

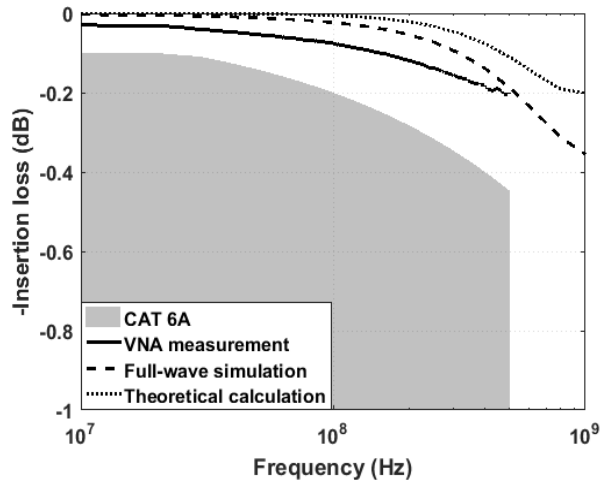

(b)

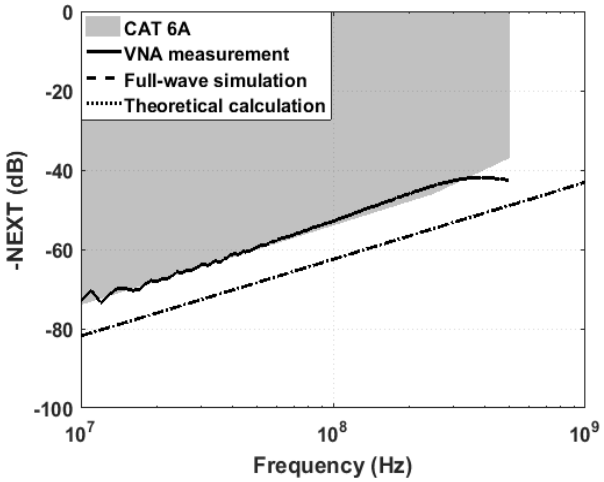

(c)

Fig 13. Results of theoretical approach and 3D full wave simulation compared with VNA measurement for the optimized prototype. (a) Return loss; (b) Insertion loss; (c) NEXT

VI. Conclusion

This paper presented a theoretical analysis of coupled differential pairs for interconnection applications, which led to predict the value of coupling coefficient allowing to meet the limit of crosstalk for Ethernet category 6A. Two modeling methods have been proposed and validated by measurements. A 2D modeling approach using segmentation enabled optimization of the impedance matching along the contact. The optimization process also took into account the best compromise between adaptation, crosstalk level and mounting issues. The design and the materials of the optimized contact are compatible with harsh environments and data rates of 10 Gbits/s are reachable.

Acknowledgment

The authors would like to thank the Region Auvergne-Rhone-Alpes for the financial support inside COCHISE project and to have enabled the collaboration between IMEP-LAHC laboratory and Amphenol-Socapex.

References

[1] RS. Timsit, “High Speed Electronic Connectors: A Review of Electrical Contact Properties”, *IEICE Trans. Electron.*, vol. 88, no. 8, pp. 1532-1545, 2005.
[2] JG. Kraemer, “Specifying and characterizing cable/connector systems for high-speed interfaces in defense/aerospace systems”, *International Symposium on Electromagnetic Compatibility*, vol. 3, pp. 943-948, EMC 2005.
[3] NF EN 3155-074 and NF EN 3155-075
[4] ISO/IEC 11 801:2010
[5] Ungerboeck, Gottfried. “10GBASE-T Coding and Modulation: 128-DSK+LDPC.” IEEE P802. 3an Task Force, Ottawa, Sep: 15.
[6] VK. Tripathi, “Asymmetric coupled lines in a inhomogeneous medium”, *IEEE Trans. Microw. Theory Tech.*, vol. 3, no. 9, pp. 734-739, 1975.
[7] DE. Bockelman, WR. Eisenstadt, “Combined differential and common-mode scattering parameters: Theory and simulation”, *IEEE Trans. Microw. Theory Tech.*, vol. 43, no. 7, pp. 1530-1539, 1995.
[8] WR. Eisenstadt, Y. Eo, “S-parameter-based IC interconnect transmission line characterization”, *IEEE Trans. Comp. Hybrids, Manuf. Technol.*, vol. 15, no. 4, pp. 483-490, 1992.
[9] AA. Bhatti, “A computer based method for computing the N-dimensional generalized ABCD parameter matrices of N-dimensional systems with distributed parameters”, *The Twenty-Second Southeastern Symposium on System Theory*, pp. 590-593, January 1990.
[10] DA. Frickey, “Conversions between S, Z, Y, H, ABCD, and T parameters which are valid for complex source and load impedances”, *IEEE Trans. Microw. Theory Tech.*, vol. 42, no. 2, pp. 205-211, 1994.
[11] MK. Sampath, “On addressing the practical issues in the extraction of RLGC parameters for lossy multiconductor transmission lines using S-parameter models”. *IEEE-EPEP Elect. Perform. Electron. Packag.*, pp. 259-262, 2008.

Younes Boujmad received an engineering degree in electronic and telecommunication from ENSIL, Limoges, France in 2017 and is preparing a PHD at IMEP-LAHC Laboratory of the University of Savoie Mont Blanc, Chambery, France. His research topics are focused on interconnection design, HF measurement techniques and materials characterization.

Philippe Artillan received the Ph.D. from the Université de Toulouse in 2008. He joined the Characterization and Microwave Laboratory (IMEP-LAHC) at University of Savoie Mont Blanc, France, as an Associate Professor with the Radio Frequency and Millimeter-Wave Group. His current research interests include integrated passive components for 3-D integration technologies, with particular interest in electromagnetic modeling, broadband characterization, and material parameters extraction.

Cédric Bermond received the PhD degree in Electronic, Optronic and Systems from the University of Savoie, France, in 2001. He is an assistant professor in the Characterization and Microwave Laboratory (IMEP-LAHC) at University of Savoie Mont Blanc, France. His research interests include materials characterization for integrated components, microwave characterization, modeling and design of interconnects and passive components in advanced integrated circuits.

Bernard Fléchet received the PhD degree in Optic, Optoelectronic and Microwave from the National Polytechnic Institute of Grenoble, France, in 1991. He is a Professor in the Characterization and Microwave Laboratory (IMEP-LAHC) and director of the Electrical Engineering Department of University of Savoie, France. His research interests include modeling and design of interconnects and passive components in advanced integrated circuits.